Characterization of purified human B^{act} spliceosomal complexes reveals compositional and morphological changes during spliceosome activation and first step catalysis

SERGEY BESSONOV,[1] MARIA ANOKHINA,[1] ANDRIUS KRASAUSKAS,[2] MONIKA M. GOLAS,[2,4] BJOERN SANDER,[2,5] CINDY L. WILL,[1] HENNING URLAUB,[3] HOLGER STARK,[2] and REINHARD LÜHRMANN[1]

[1]Department of Cellular Biochemistry, MPI of Biophysical Chemistry, D-37077 Göttingen, Germany
[2]Research Group of 3D Electron Cryomicroscopy, MPI of Biophysical Chemistry, D-37077 Göttingen, Germany
[3]Bioanalytical Mass Spectrometry Group, MPI of Biophysical Chemistry, D-37077 Göttingen, Germany

ABSTRACT

To better understand the compositional and structural dynamics of the human spliceosome during its activation, we set out to isolate spliceosomal complexes formed after precatalytic B but prior to catalytically active C complexes. By shortening the polypyrimidine tract of the PM5 pre-mRNA, which lacks a 3′ splice site and 3′ exon, we stalled spliceosome assembly at the activation stage. We subsequently affinity purified human B^{act} complexes under the same conditions previously used to isolate B and C complexes, and analyzed their protein composition by mass spectrometry. A comparison of the protein composition of these complexes allowed a fine dissection of compositional changes during the B to B^{act} and B^{act} to C transitions, and comparisons with the *Saccharomyces cerevisiae* B^{act} complex revealed that the compositional dynamics of the spliceosome during activation are largely conserved between lower and higher eukaryotes. Human SF3b155 and CDC5L were shown to be phosphorylated specifically during the B to B^{act} and B^{act} to C transition, respectively, suggesting these modifications function at these stages of splicing. The two-dimensional structure of the human B^{act} complex was determined by electron microscopy, and a comparison with the B complex revealed that the morphology of the human spliceosome changes significantly during its activation. The overall architecture of the human and *S. cerevisiae* B^{act} complex is similar, suggesting that many of the higher order interactions among spliceosomal components, as well as their dynamics, are also largely conserved.

Keywords: pre-mRNA splicing; spliceosomes; mass spectrometry; electron microscopy

INTRODUCTION

Nuclear pre-mRNA splicing is catalyzed by the spliceosome, a multimegadalton ribonucleoprotein (RNP) machine (for review, see Wahl et al. 2009). The spliceosome assembles stepwise by the temporally ordered interaction of the U1, U2, and U4/U6.U5 snRNPs with the pre-mRNA. Assembly intermediates of the human spliceosome that have been observed include the E, A, B, B^{act}, B^{*}, and C complexes (observed in the stated temporal order). In the E complex the U1 snRNP is recruited to the 5′ splice site (ss) of the pre-mRNA, U2AF binds the pre-mRNA's polypyrimidine tract (which is located just upstream of the 3′ss), and SF1 binds the branch point sequence (BPS). In the subsequently formed A complex, the U2 snRNP stably associates with the BPS. After A complex formation, the U4/U6 and U5 snRNPs are recruited as a preassembled U4/U6.U5 tri-snRNP, forming the spliceosomal B complex. Although all snRNPs are present in the B complex, it is still catalytically inactive and requires major conformational and compositional rearrangements (i.e., activation) in order to become competent to facilitate the first transesterification step of splicing. During spliceosome activation U1 and U4 are destabilized or released, giving rise to the activated spliceosome (i.e., the B^{act} complex). Subsequently, after a structural rearrangement is catalyzed by the

[4]**Present address:** The Water and Salt Research Center, Institute of Anatomy and Stereology, University of Aarhus, DK-8000 Aarhus C, Denmark.
[5]**Present address:** Electron Microscopy Laboratory, University of Aarhus, DK-8000 Aarhus C, Denmark.
Reprint requests to: Reinhard Lührmann, Department of Cellular Biochemistry, Max Planck Institute for Biophysical Chemistry, Am Fassberg 11, 37077 Göttingen, Germany; e-mail: Reinhard.Luehrmann@mpi-bpc.mpg.de; fax: 49-551-2011197.
Article published online ahead of print. Article and publication date are at http://www.rnajournal.org/cgi/doi/10.1261/rna.2456210.

DExH/D-box protein Prp2, the catalytically activated spliceosome (B* complex) is formed. The latter is then converted into the C complex, in which the first of the two catalytic steps of splicing has occurred. During the first step, the branch point adenosine of the intron carries out a nucleophilic attack on the 5′ss, resulting in cleavage of the pre-mRNA at this site and the concomitant ligation of the 5′ end of the intron to the branch point adenosine, generating a lariat-like structure. After the second step, in which the exons are ligated and the spliced intron is released, the spliceosome dissociates and the snRNPs are recycled for additional rounds of splicing.

During spliceosome assembly a dynamic network of RNA–RNA interactions involving the snRNAs and pre-mRNA is formed (for review, see Nilsen 1998; Staley and Guthrie 1998). This network plays a central role in juxapositioning the reactive groups of the pre-mRNA for catalysis. Initially, U1 and U2 snRNA base pair with the 5′ss and BPS, respectively. Within the tri-snRNP, U4 and U6 are extensively base paired. Upon addition of the tri-snRNP to the spliceosome, the U5 snRNA intially contacts nucleotides of the 5′ exon near the 5′ss, and later also the 3′ exon. Prior to the first step of splicing, the U4/U6 base pairing interaction is disrupted, and the U6 snRNA forms base pairs with intron nucleotides at the 5′ss, displacing U1 in the process. U6 also forms short duplexes with U2, and an intramolecular U6 stem–loop (U6-ISL) is formed, which is involved in metal ion binding. The RNA structures formed by U2 and U6 snRNA are thought to directly contribute to the catalysis of the splicing reaction. Additional rearrangements also occur prior to the second step of splicing (for review, see Smith et al. 2008), but they are currently not well understood.

The spliceosome possesses a very complex protein composition, and spliceosomal proteins play key roles throughout the splicing process (Jurica and Moore 2003; Wahl et al. 2009). Mass spectrometry (MS) analyses of affinity purified, human spliceosomes isolated under physiological conditions revealed that over the course of splicing ~170 proteins associate with the human spliceosome, with individual assembly intermediates (e.g., A, B, and C complexes) containing ~120 proteins or less (in the case of the A complex) (Deckert et al. 2006; Behzadnia et al. 2007; Bessonov et al. 2008). MS analyses of *Saccharomyces cerevisiae* spliceosomes revealed that they are not as complex compared with those of higher eukaryotes, with ~90 associated proteins (Fabrizio et al. 2009). This lower complexity appears to reflect the near absence of regulated/alternative splicing in yeast, as many of the spliceosomal proteins found solely in metazoan spliceosomes are involved in alternative/regulated splicing events. Despite the aforementioned differences between yeast and human spliceosomes, homologs of nearly all proteins present in the yeast spliceosome are also found in human spliceosomes (Fabrizio et al. 2009), indicating that the core splicing machinery is evolutionarily conserved.

A comparison of the composition of A, B, and C spliceosomal complexes revealed that there is a dramatic exchange of proteins during spliceosome assembly/catalytic activation in both humans and *Drosophila melanogaster* (Deckert et al. 2006; Bessonov et al. 2008; Herold et al. 2009). During the transitions from the A to B and B to C complex a large number of proteins are recruited, and at the same time numerous spliceosomal proteins are released or destabilized (for review, see Wahl et al. 2009). These compositional dynamics are also for the most part conserved in *S. cerevisiae*, where the changes in protein composition accompanying the B to B^{act} and B^{act} to C complex transitions were recently elucidated (Fabrizio et al. 2009).

Activation of the spliceosome is a decisive step that involves major structural changes. The destabilization/dissociation of both U1 and U4 snRNA is a hallmark of the activation process. Proteins of the DExH/D-box family of RNA/RNP unwindases are the main driving forces that mediate RNA rearrangements at this step. For example, Prp28/U5-100K catalyzes the exchange of U6 for U1 at the 5′ss (Staley and Guthrie 1999; Chen et al. 2001), whereas Brr2/U5-200K, together with the GTPase Snu114, facilitates U4/U6 unwinding (Laggerbauer et al. 1998; Raghunathan and Guthrie 1998; Bartels et al. 2002; Brenner and Guthrie 2005; Small et al. 2006). The Prp19 protein, in the form of a heteromeric protein complex (the nineteen complex or NTC in yeast and the Prp19/CDC5L complex in humans) plays an essential role in spliceosome activation (Chan et al. 2003; Makarova et al. 2004). The NTC complex acts subsequent to U4 dissociation, stabilizing the association of U5 and U6 with the activated spliceosome (Chan et al. 2003) and specifying the proper interaction of U5 and U6 with the pre-mRNA substrate prior to step 1 (Chan and Cheng 2005).

While spliceosome activation is well characterized at the RNA level, changes in the spliceosome's protein composition and morphology, as well as RNP remodeling events accompanying activation, are not completely understood. All U1- and U4/U6-associated proteins are destabilized or released from the human spliceosome during the B to C complex transition, together with a number of other spliceosomal proteins (Bessonov et al. 2008). Whether these proteins are destabilized/released concomitantly or in discrete steps, in particular during the B to B^{act} or B^{act} to C complex transition, is presently not entirely clear in higher eukaryotes, as activated human spliceosomes have to date not been isolated under physiological conditions. In previous studies, human spliceosomes that had undergone activation were isolated under stringent conditions in the presence of heparin, and thus only those proteins stably associated with the spliceosome at this stage could be identified (Makarov et al. 2002). Comparisons with B and C complexes isolated under stringent conditions were hampered by the use of different pre-mRNA substrates and the fact that different methods were used to purify each of these complexes (Jurica et al. 2002; Makarov et al. 2002; Makarova et al. 2004). Nonetheless, these studies indicate that U1- and U4-associated proteins are destabilized upon activation, and proteins

of the Prp19/CDC5L complex, and those operationally defined as Prp19-related, appear to stably interact with the spliceosome first at the time of its activation (Makarova et al. 2004). As the U6 snRNA has been "stripped" of all of its precatalytic binding partners during spliceosome activation, it must be remodeled and engage in interactions with new protein binding partners (Wahl et al. 2009). In humans there is evidence that the U5 snRNP is also remodeled during activation; ~15 proteins, including those comprising the human Prp19/CDC5 complex, associate stably with U5 at this stage, yielding a remodeled 35S form of the U5 snRNP (Makarov et al. 2002). The yeast helicase Prp2 and its binding partner Spp2 both play a crucial role in spliceosome activation (Roy et al. 1995; Kim and Lin 1996; Silverman et al. 2004), with Prp2 activity promoting a poorly understood remodeling event that converts B^{act} into the catalytically active B^* complex (Kim and Lin 1996; Warkocki et al. 2009).

To learn more about the compositional and structural dynamics of the human spliceosome during the B to B^{act} and B^{act} to C complex transitions, here we have affinity-purified human B^{act} complexes under physiological conditions identical to those used previously to isolate human B and C complexes, and determined their protein composition via mass spectrometry. Morphological changes occurring during spliceosome activation were also elucidated by performing electron microscopy of purified B^{act} complexes and comparing their 2D EM structure with that of human B complexes. A comparison of the composition and morphology of human and yeast B^{act} complexes revealed that the compositional and structural dynamics accompanying spliceosome activation are largely conserved between yeast amd metazoans. These studies provide new insights into the recruitment and release of proteins during the activation of the human spliceosome and the accompanying changes in its structure at this stage.

RESULTS

PM5 pre-mRNA with a truncated polypyrimidine tract supports spliceosome formation but not step I catalysis

To gain a better understanding of the spliceosome activation process, we set out to purify spliceosomal complexes stalled after activation, but prior to the first catalytic step of splicing, under conditions used previously for the isolation of human B and C complexes (Bessonov et al. 2008). In yeast, truncation of an actin pre-mRNA substrate to within a few nucleotides of the branch site stalls spliceosome assembly at the B^{act} stage (Cheng 1994; Fabrizio et al. 2009). We thus first tested whether shortening the polypyrimidine tract of the PM5 pre-mRNA substrate, which was used to purify human B and C complexes (Bessonov et al. 2008), would also stall human spliceosomes at the B^{act} complex stage. The PM5 pre-mRNA contains a 5′ exon, an intron with a branch site and a 60-nucleotide (nt) long polypyrimidine tract, but no terminal AG dinucleotide and no 3′ exon (Fig. 1A). Due to the absence of the 3′ss and 3′ exon, the second step of splicing does not occur with the PM5 substrate. For affinity purification, three RNA aptamers that bind the MS2 coat protein were added to the 5′ end of the PM5 substrate.

We sequentially shortened the polypyrimidine tract of the PM5 pre-mRNA and assayed whether splicing in HeLa nuclear extracts was affected. Shortening the polypyrimdine tract from 60 to 30 or 28 nt did not affect the efficiency of the first step of splicing, as splicing intermediates were formed with nearly equal efficiency after 15 and 60 min in each case (Fig. 1B, lanes 13–21). However, truncation to 26 nt or less severely inhibited step 1 (Fig. 1B, lanes 1–12; Fig. 1D). Splicing was completely abolished, even after longer incubation times (90 min), when the PPT was shortened to 20 (designated PM5–20) or 10 nt (PM5–10) (Fig. 1D). Native gel analysis of splicing complex formation demonstrated that A and B complexes form rapidly on the PM5 substrate (Fig. 1C,E), whereas C complexes are observed first after 15 min, concomitant with the appearance of the splicing intermediates. The PM5 spliceosomal complexes first observed after 15 min that migrate above the B complex run as a diffuse band, suggesting this might be a mixture of B^{act} complexes and C. Strikingly, upon shortening the PPT to 26 nucleotides (or less), a single discrete band that migrates slower than the C complex is observed (Fig. 1C). As it appears concomittant with the reduction/loss of step I of splicing, it likely represents the B^{act} complex. This complex was also detected with the PM5–20 and PM5–10 pre-mRNAs, where after 90 min predominantly it (and essentially no A/B complexes) plus low levels of E/H complexes were observed. Formation of this complex, together with that of A and B complexes, was abolished if the PM5 PPT was completely deleted (Fig. 1E). Taken together, these data indicate that human spliceosomal complexes likely representing activated B complexes can be assembled in vitro using a pre-mRNA substrate where the PPT is shortened to ~20 nt.

Affinity purification of the human-activated B complex

To isolate these putative B^{act} complexes, MS2-affinity purifications were performed. For this purpose, ^{32}P-labeled PM5–20 and PM5–10 pre-mRNA were preincubated with MS2–MBP fusion protein and splicing complexes were then allowed to form by incubating in HeLa nuclear extract under splicing conditions for 2.5 h. Pre-mRNA not incorporated in B^{act} complexes was digested by DNA oligonucleotide-directed RNase H digestion using an oligonucleotide directed against the 3′ end of the 5′ exon; this region is protected in B^{act} complexes, but not in A and B complexes (data not shown). Splicing reactions were then subjected to glycerol gradient centrifugation to separate the B^{act} complexes from

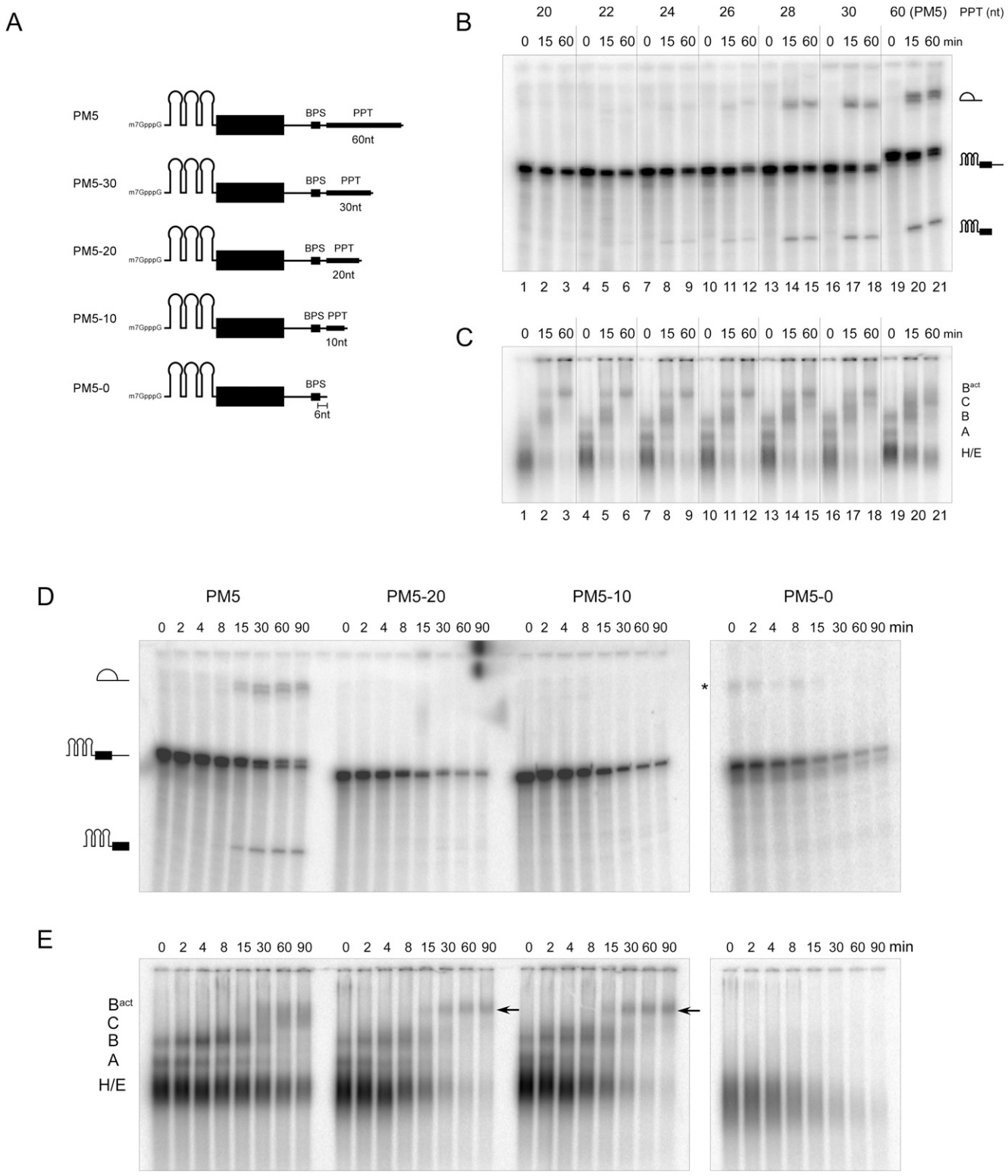

FIGURE 1. Truncation of the polypyrimidine tract (PPT) stalls splicing prior to the first catalytic step. (*A*) Schematic of PM5 pre-mRNA constructs used, where the polypyrimidine tract was truncated to the indicated length. All constructs have a 6-nt stretch between the branch point adenosine and PPT. Kinetics of in vitro splicing (*B,D*), and splicing complex formation (*C,E*) with the PM5 pre-mRNA and truncated versions thereof. Pre-mRNAs were incubated under splicing conditions in the presence of HeLa nuclear extract for the times indicated above each lane. RNA was analyzed by denaturing PAGE and visualized by autoradiography (*B,D*) The pre-mRNA and splicing intermediates are indicated on the *right* or *left*. Spliceosomal complex formation was assayed on a native agarose gel. The positions of the H/E, A, B, C, and B^{act} complexes are indicated. The arrow indicates the position of the B^{act} complex. Asterisk, unknown contaminating band.

excess of MS2–MBP protein, RNase H digestion fragments, and other smaller spliceosomal complexes. Two peaks containing the ^{32}P-labeled PM5–20 or PM5–10 (not shown) pre-mRNA were observed, a minor one peaking in fraction 13 and a major one in fraction 19, with S values of ~32 and ~45, respectively (Fig. 2A, and data not shown). The former contains the products of RNase H digestion, and the latter the B^{act} complex.

Complexes in the 45S peak fractions were pooled and incubated with amylose agarose beads. After extensive washing, bound complexes were eluted with maltose and their RNA composition was analyzed by denaturing PAGE, followed by autoradiography and silver staining. As shown in Figure 2B, the affinity purified 45S spliceosomal complexes contained nearly equimolar amounts of unspliced PM5–10 or PM5–20 pre-mRNA and U2, U5, and U6 snRNA (lanes 3 and 4), and only very small amounts of U1 and U4 snRNA, indicating that the vast majority have undergone activation. Importantly, no splicing intermediates were detected, even by autoradiography (lanes 1 and 2), indicating that no C complexes had been isolated. Taken together, these results indicate that human B^{act} complexes of relatively high purity were isolated.

Protein composition of human B^{act} complexes

To determine the composition of B^{act} complexes formed on both the PM5–10 and PM5–20 pre-mRNA, proteins present in affinity-purified complexes were separated by SDS-PAGE and stained with Coomassie (Fig. 2C). Proteins present in the B^{act} complex were identified by liquid chromatography tandem mass spectrometry (LC-MS/MS), and the number of peptides sequenced for each protein identified is summarized in Table 1. For comparison, proteins previously identified in affinity purified human B complexes formed on PM5 pre-mRNA (plus the number of peptides sequenced) are also shown in Table 1. In addition, we affinity-purified C complexes formed on the PM5 pre-mRNA as previously described (Bessonov et al. 2008) or on the MINX pre-mRNA containing an AG to GG mutation at the 3′ss (denoted $MINX_{GG}$), which stalls spliceosomes at the C complex stage (data not shown; Golas et al. 2010) and performed LC-MS/MS in parallel with the purified B^{act} complexes.

Over 140 proteins, including both snRNP and non-snRNP proteins, were reproducibly identified in our purified B^{act} complex preparations, with complexes formed on PM5–20

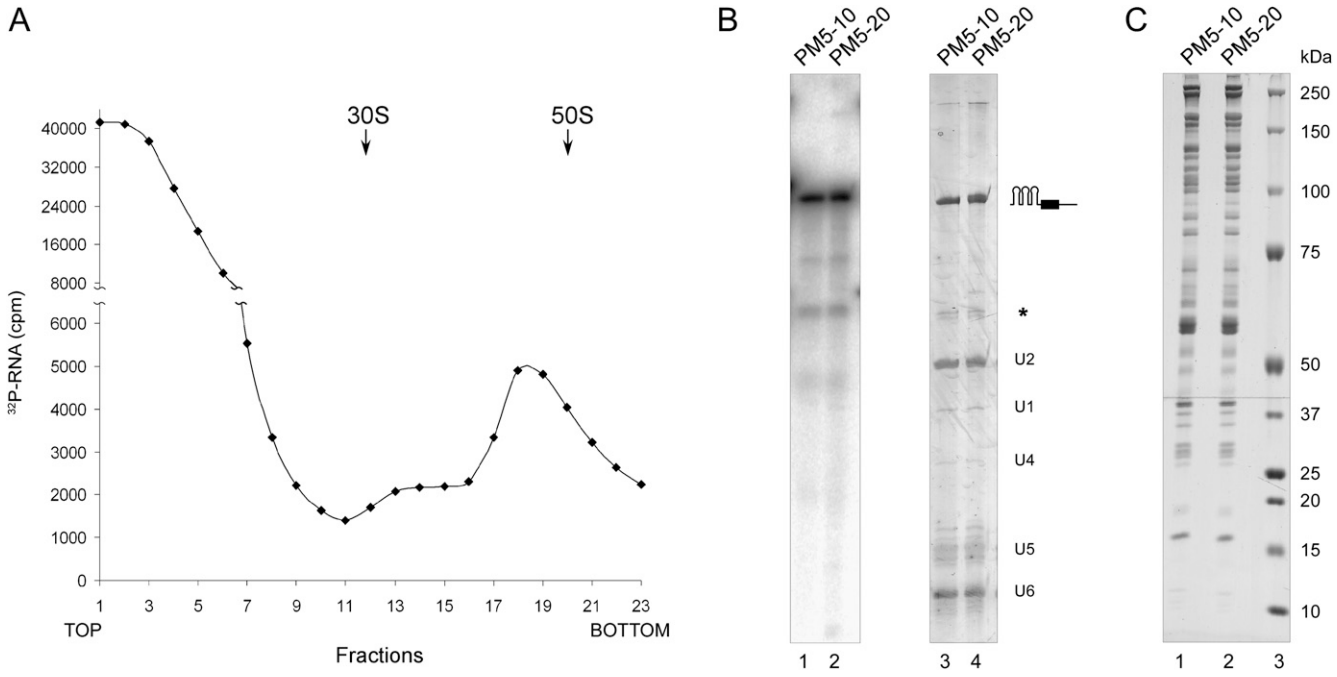

FIGURE 2. Affinity purification of human, spliceosomal B^{act} complexes. (*A*) Glycerol gradient fractionation of splicing complexes formed on the PM5-20 construct. In vitro splicing, followed by RNAse H digestion, was performed as described in the Materials and Methods. Complexes were then separated on a linear 10%–30% glycerol gradient and the ^{32}P-RNA in each fraction was determined by Cherenkov counting. S-values were determined by comparison with a reference gradient containing prokaryotic ribosomal subunits. Gradient profiles for both PM5-10 (not shown) and PM5-20 complexes were identical. (*B,C*) Composition of affinity-purified complexes. Gradient fractions containing 45S complexes (fractions 17–21) were pooled and subjected to MS2 affinity selection. (*B*) RNA was recovered, separated by denaturing PAGE, and visualized by autoradiography (lanes *1* and *2*) and by silver staining (lanes *3* and *4*). The positions of the snRNAs and the PM5-20 and PM5-10 pre-mRNA are indicated on the *right*. Asterisk, RNase H degradation product. The other minor bands seen in lanes *1* and *2* do not correspond to splicing intermediates, but are likely degradation products. (*C*) Protein was recovered from the affinity purified B^{act} complexes (lanes *1* and *2*), analyzed by SDS-PAGE on an 8%/14% polyacrylamide step gel, and visualized by staining with Coomasie. The size of molecular weight markers (lane *3*) is indicated on the *right*.

TABLE 1. Protein composition of affinity-purified human B^{act} complexes

Protein	GenBank accession no.	kDa	B	B	B^{act} PM5-10	B^{act} PM5-20	C MINX-GG	C PM5	Yeast B^{act}	*S. cerevisiae* gene name
Sm proteins										
B	gi|4507125	24.6	34	22	36	45	31	18	•	*SMB1*
D1	gi|5902102	13.3	18	20	20	15	9	3	•	*SMD1*
D2	gi|29294624	13.5	24	60	74	48	52	34	•	*SMD2*
D3	gi|4759160	13.9	22	35	38	35	15	17	•	*SMD3*
E	gi|4507129	10.8	24	23	18	12	14	6	•	*SME1*
F	gi|4507131	9.7	21	23	9	5	6	6	•	*SMX3*
G	gi|4507133	8.5	7	11	8	5	8	5	•	*SMX2*
U1 snRNP										
U1-70K	gi|29568103	51.6		11	3		2	2		*SNP1*
U1-A	gi|4759156	31.3	17	8	3	3	1		•	*MUD1*
17S U2 snRNP										
U2A′	gi|50593002	28.4	55	12	85	62	74	32	•	*LEA1*
U2B″	gi|4507123	25.4	25	15	33	27	30	20	•	*MSL1*
SF3a120	gi|5032087	88.9	84	47	111	125	39	40	•	*PRP21*
SF3a66	gi|21361376	49.3	18	25	30	10	9	4	•	*PRP11*
SF3a60	gi|5803167	58.5	39	42	74	72	30	32	•	*PRP9*
SF3b155	gi|54112117	145.8	153	119	208	194	75	54	•	*HSH155*
SF3b145	gi|55749531	100.2	82	61	136	118	31	36	•	*CUS1*
SF3b130	gi|54112121	135.5	209	254	351	336	105	98	•	*RSE1*
SF3b49	gi|5032069	44.4	8	1	9	10	3	4	•	*HSH49*
SF3b14a/p14	gi|7706326	14.6		17	29	29	11	6		
SF3b14b	gi|14249398	12.4	19	22	17	18	7	5	•	*RDS3*
SF3b10	gi|13775200	10.1		7	6	7	2	2	•	*YNL138W-A/RCP10/YSF3*
17S U2 related										
HPRP43	gi|68509926	90.9	51	54	27	23	45	28		*PRP43*
U2AF65	gi|6005926	53.5	8	4						
SPF45	gi|14249678	45	19	9	1	4	2			
SR140(fSAPa)	gi|122937227	118.2	34	17	5	5	4			
CHERP	gi|119226260	100	14	7						
SF3b125	gi|45446747	103	29	10						
U5 snRNP										
220K	gi|3661610	273.7	408	335	523	704	556	451	•	*PRP8*
200K	gi|45861372	244.5	267	375	542	623	490	370	•	*BRR2*
116K	gi|41152056	109.4	169	168	335	354	245	198	•	*SNU114*
40K	gi|4758560	39.3	23	37	48	32	60	47		
102K	gi|40807485	106.9	90	170	68	63	40	53		*PRP6*
15K	gi|5729802	16.8	6	11						
100K	gi|41327771	95.6	47	107	36	39	47	53		*PRP28*
52K	gi|5174409	37.6	18	5	4	5	8	6		*LIN1(SNU40)*

(*continued*)

TABLE 1. *Continued*

Protein	GenBank accession no.	kDa	B	B	B^{act} PM5-10	B^{act} PM5-20	C MINX-GG	C PM5	Yeast B^{act}	*S. cerevisiae* gene name
LSm proteins										
LSm2	gi|10863977	10.8	20	10				1		*LSM2*
LSm3	gi|7657315	11.8		3	2	3				*LSM3*
LSm4	gi|6912486	15.4	13	19						*LSM4*
LSm6	gi|5919153	9.1		12	1				•	*LSM6*
LSm7	gi|7706423	11.6	10	5						*LSM7*
LSm8	gi|7706425	10.4	10	18	3	2	1			*LSM8*
U4/U6 snRNP										
90K	gi|4758556	77.6	63	75	3		17	13		*PRP3*
60K	gi|45861374	58.4	37	57	11	3	11	8		*PRP4*
20K	gi|5454154	20	24	14	1		2			*CPRS or CPR3*
61K	gi|40254869	55.4	27	60	10		10	7		*PRP31*
15.5K	gi|4826860	14.2	7	9		1				*SNU13*
U4/U6.U5 tri-snRNP										
110K	gi|13926068	90.2	65	57	13	7		14		*SNU66*
65K	gi|56550051	65.4	26	48	18	26	22	23		*SADI*
HPRP38	gi|24762236	37.5	17	30	23	31	8	3	•	*PRP38*
hPRP19/CDCSL complex										
hPRP19	gi|7657381	55.2	39	96	167	173	146	152	•	*PRP19*
CDCSL	gi|11067747	92.2	70	53	266	336	240	240	•	*CEF1*
SPF27	gi|5031653	21.5	21	11	39	41	50	27	•	*SNT309*
PRL1	gi|4505895	57.2	22	28	115	88	72	60	•	*PRP46*
CCAP1(hsp73)	gi|5729877	70.4		8	24	23			•	*Ssa/Ssb families*
CCAP2(hspc148, AD-002)	gi|7705475	26.6	10	1	23	25	36	20	•	*CWC15*
catenin, β-like 1 (CTNNBL1, NAP)	gi|18644734	65.1	21	13	43	41	7	10		
Npw38BP	gi|7706501	70	17	10	17	13	4			
Npw38	gi|5031957	30.5			4	3				
hPRP19/CDC5L related										
PRCC	gi|40807447	52.4	9		2	4				
RBMM22 (fSAP47)	gi|8922328	46.9	29	11	86	97	90	46	•	*CWC2 + ECM2*
hSYF1 (XAB2)	gi|55770906	100	53	36	288	318	214	211	•	*SYF1*
CRNKL1 (hSYF3)	gi|30795220	100.6	66	86	186	263	126	150	•	*CLF1*
hIsy1 (fSAP133)	gi|20149304	33	19	4	39	27	40	25	•	*ISY1*
SKIP	gi|6912676	51.1	37	60	195	275	229	132	•	*PRP45*
Cyp-E	gi|5174637	33.4	13	6	53	47	68	30		
PPIase-like 1 (PPIL1)	gi|7706339	18.2	7	15	7	19	16	16		
KIAA0560 (fSAP164)	gi|38788372	171.3	41	44	318	356	284	219		*SEN1*
G10 (fSAP17)	gi|32171175	17	9	10	9	14	29	13	•	*BUD31/CWC14*
Recruited prior to B^{act} complex										
TCERG1 (CA150)[a]	gi|21327715	123.9		4	11	10				*YPR152C,URN1*
NRIP2[a]	gi|13899327	31.3			1	1				

(*continued*)

TABLE 1. *Continued*

Protein	GenBank accession no.	kDa	B	B	B^{act} PM5-10	B^{act} PM5-20	C MINX-GG	C PM5	Yeast B^{act}	*S. cerevisiae* gene name
FBP11[a]	gi|151301228	105.8		7			7	1		
DDX9	gi|4503297	142		14	2					
p72 (DDX17)	gi|3122595	80.5	6	23		1	2	3		*DBP2*
RNPC2(CC1.3, CAPER, FSAP59)	gi|4757926	58.5	10	48	8	10				
hsp27	gi|4504517	22.8	6	3	3	6	8	7		
MFAP1	gi|50726968	51.9	37	49	41	36	19	13		
RED	gi|10835234	65.6	43	58	29	15	14	10		
hSmu-1 (fSAP57)	gi|8922679	57.5	47	79	29	25	18	9		
UBL5	gi|13236510	8.5	2	10	1	2	1			*HUB1*
hPRP4-Kinase	gi|89276756	117.1	19	34	11	13	21	36		*YAK1*
HsKin17	gi|13124883	45.4	18	10	12	8	11	1		*RTS2*
BCLAF1	gi|7661958	106	25	34	18	14	17	34		
SKIV2L2(fSAP118, KIAA0052)	gi|193211480	117.8	18	9	14	11	23	24		*MTR4*
THRAP3 (TRAP150)	gi|167234419	108.5	42	48	15	21	11	18		
Abundant first in B^{act} complex										
KIAA1604 (fSAPb)	gi|55749769	105.5	42	8	159	158	191	150	•	*CWC22*
hPRP17	gi|7706657	65.5	19	21	105	147	140	110	•	*CDC40*
hPRP2	gi|4503293	119.2	38	12	157	136	56	65	•	*PRP2*
GPKOW (T54, GPATC5)	gi|15811782	52.1			39	47	20	23	•	*SPP2*
NY-CO-10	gi|64276486	53.8	8	6	58	54	11	19	•	*CWC27*
RNF113A	gi|5902158	38.8	9	1	39	43	11	13	•	*CWC24*
MGC20398	gi|49472814	42	22	3	41	27	14	20		
PPIL2 (Cyp-60)	gi|7657473	59.5	22	26	59	62	22	27		
MGC23918	gi|21389497	19.2	18	7	33	30	18	20		
FRG1	gi|4758404	29.2			21	24	14	13		
Detected in B^{act} complex										
p30 DBC	gi|24432106	102.8			2	2				
FAM58A	gi|196049384	26			2	3				
NCOR1	gi|22538461	270.1			2	1				*SNT1*
TRIM24(TIF1, PTC6, RNF82)	gi|47419911	116.7			2	3				
LENG1	gi|24308289	30.4			2	3				
DDX50	gi|13129006	82.4			5	7				
FLJ38348	gi|167900474	30.1			4	2				
CRIPT (HSPC139)	gi|7661798	11.1			10	10				
GTL3	gi|8392875	22.6			1	2				
MOV10	gi|14211540	113.5			3	2				
FUBP3	gi|100816392	61.5			6	7				
2nd step factors										
hPRP22	gi|4826690	139.3		7	6	15	224	211		*PRP22*
hPRP16	gi|17999539	140.5				1	26	7		*PRP16*
hSLU7	gi|27477111	68.4				2	94	72		*SLU7*

(*continued*)

TABLE 1. *Continued*

Protein	GenBank accession no.	kDa	B	B	B^{act} PM5-10	B^{act} PM5-20	C MINX-GG	C PM5	Yeast B^{act}	*S. cerevisiae* gene name
Abundant first in C complex										
Abstrakt	gi|21071032	69.8		3	1	4	228	180		
HSP70	gi|5123454	70	17	8			30	20	•	*Ssa/Ssb families*
PPWD1 (KIAA0073, CyP64)	gi|24308049	73.6				1	69	43		
PPIase-like 3b	gi|19557636	18.6				2	19	10		
GCIP p29 (fSAP29)	gi|46371998	28.7			14	11	74	31	•	*SYF2*
DDX35	gi|20544129	78.9		7	9	23	31	34		
C19orf29(NY-REN-24, cactin)	gi|126723149	88.6				1	66	71		
PPIG (SRcyp)	gi|42560244	88.5		2	1	1	24	29		
C10orf4(LOC118924, FRA10AC1)	gi|24432067	37.5				3	33	19		
C1orf55 (FLJ 35382)	gi|148664216	39.3					46	29		
C9orf78(HSPC220, LOC51759)	gi|7706557	33.7					10	12		
DGCR14	gi|13027630	52.4				1	62	43		
DKFZP586O0120 (FAM32A)	gi|7661696	13.1				3	28	21		
FAM50A (HXC-26, XAP5)	gi|4758220	40.1					48	24		
FAM50B	gi|6912326	38.6					7	5		
CXorf56 (FLJ22965)	gi|11545813	25.6				3	52	22		
NFKBIL1 (IKBL)	gi|26787991	43.1					21	12		
NKAP	gi|13375676	47					12	9		
TTC14	gi|33457330	88.2					21	24		
NOSIP	gi|7705716	33.2					24	17		
CDK10	gi|16950647	35.4					22	12		
PRKRIP1 (C114, FLJ13902)	gi|13375901	20.9				1	19	20		
Q9BRR8	gi|74732921	103.3				1	29	25		
ZCCHC10	gi|8923106	19.3					14	9		
TFIP11	gi|8393259	96.8		12	11	8	22	26		*SPP382/YLR424W/NTR1*
MORG1	gi|153791298	34.3		1	2	1	12	11		
Detected in C complex										
eIF3 S6	gi|7705433	66.6					6	2		
WDR70	gi|8922301	73.1					7	2		
RBM4	gi|93277122	40.2					4	4		
BCAS1 (AIBC1, NABC1)	gi|191251777	61.2					1	2		
DBPA	gi|20070160	40.1		1		6	4	1		
matrin 3	gi|21626466	94.6		3			11	3		*ECM13*
EJC/mRNP										
eIF4A3	gi|7661920	46.9	27	18	51	52	94	75		*FAL1*
Magoh	gi|4505087	17.2		4			15	7		
Y14	gi|4826972	19.9	4	2	3	3	9	7		
Pinin	gi|33356174	81.6		11		1	18	23		
RNPS1	gi|6857826	34.2		6	1	1	10	12		
Acinus (fSAP152)	gi|7662238	151.8	44	33	11	5	33	57		
SAP18	gi|5032067	18.4	10	6	3		5	6		
Aly/REF (THOC4)	gi|55770864	26.9		5		2	4	6		*YRA1*

(*continued*)

TABLE 1. *Continued*

Protein	GenBank accession no.	kDa	B	B	B^{act} PM5-10	B^{act} PM5-20	C MINX-GG	C PM5	Yeast B^{act}	*S. cerevisiae* gene name
UAP56	gi|18375623	49.1	11	21	2	1	6	11		*SUB2*
ELG	gi|8923771	38.9	8	4	5	2	5	7		
DDX3	gi|87196351	73.3	24	9	2	2	2	11		*DED1 or DBP1*
mRNA binding proteins										
PABPC4 (IPABP, APP1)	gi|4504715	70.6		6			4	3		
PABP1	gi|46367787	70.5	29	16	5	5	8	7		*PAB1*
PABPN1 (PAB2, OPMD)	gi|4758876	32.6	4	5	4	5	8	4		
YB-1	gi|34098946	35.9	10	15	30	38	13	25		
ASR2B	gi|33383233	100	31	20	14	15	25	56		
p68 (DDX5)	gi|4758138	69.2	14	14	7	14	16	14		*DBP2*
ELAV (HuR)	gi|38201714	36.1	52	77	1	2	9	10		
NF45	gi|24234747	43	12	10		4	5	5		
LOC124245	gi|31377595	104	28	4	7	9	14	14		
cap binding complex										
CBP20	gi|110349727	18	14	25	6	23	22	19		*CBC2*
CBP80	gi|4505343	91.8	47	95	103	90	61	98		*STO1*
TREX										
THOC1 (HPR1)	gi|154448890	75.6	12	5	7	5	7	11		*HPR1*
THOC2	gi|125656165	169.6		2	3	4	12	12		*RLR1*
THOC3	gi|14150171	38.8	7		2	1	2	4		*TEX1/YNL253W*
THOC5 (KIAA0983, fSAP79)	gi|50959110	78.5		10	8	4	3	10		
THOC6 (WDR58, MGC2655)	gi|31543164	37.5		2	2	2	1	6		
THOC7 (FLJ23445, fSAP24)	gi|13376623	23.7	11			2	1	4		
RES complex										
SNIP1	gi|21314720	45.8	10	12	57	50	10	10	•	*YLR016C/PML1*
MGC13125 (fSAP71)	gi|14249338	70.5	44	17	78	108	21	23	•	*BUD13*
CGI-79	gi|4929627	39.7		6	9	10	10	10	•	*IST3/SNU17*
SR proteins										
SF2/ASF	gi|5902076	27.8	42	18	24	29	28	42		
9G8	gi|72534660	27.4	57	76	26	27	28	27		
SRp20	gi|4506901	19.4	15	18	2	5	5	4		
SRp30c	gi|4506903	25.5	32	23	38	49	20	44		
SRp38	gi|5730079	31.3	18	27	39	39	5	44		
SRp40	gi|3929378	31.3	24	21	4	5	2	15		
SRp55	gi|20127499	39.6	20	23	6	9	10	34		
SRp75	gi|21361282	56.8		3			3	3		
hTra-2 alpha	gi|9558733	32.7	16	18	6	9	5	18		
hTra-2 beta (SFRS10)	gi|4759098	33.7	21	32	8	13	9	24		
SR related proteins										
SRm160	gi|42542379	102.5		2	15	22	6	8		
SRm300	gi|4759098	300	52		189	241	194	145	•	*CWC21*

(*continued*)

TABLE 1. *Continued*

Protein	GenBank accession no.	kDa	B	B	B^{act} PM5-10	B^{act} PM5-20	C MINX-GG	C PM5	Yeast B^{act}	*S. cerevisiae* gene name
hnRNP										
hnRNP A1	gi|4504445	38.7	11	19	3	3	3	7		
hnRNP A3	gi|34740329	39.6		15		1	3	4		
hnRNP AB	gi|12803583	36	5	7			1	2		
hnRNP A2/B1	gi|14043072	37.4	15	20			1	2		
hnRNP C	gi|4758544	33.3	43	51	10	6	27	52		
hnRNP D	gi|14110420	38.4		3			1	1		
hnRNP F	gi|148470406	45.7		2	1		3	3		
hnRNP G	gi|56699409	42.4	35	34	39	46	15	33		
hnRNP H1	gi|5031753	49.1		5	2	2	4	5		
hnRNP K	gi|14165435	51	17	12		1				
hnRNP M	gi|14141152	77.5	31	32	7	6	14	25		
hnRNP Q	gi|15809590	69.6	15	6	1	2				
hnRNP R	gi|5031755	70.9		22	6	10	11	17		
hnRNP U	gi|14141161	90.6	14	4						
PCBP1	gi|5453854	37.5	13	42	4	4	5	6		*HEK2*
PCBP2	gi|14141166	38.1	15				3	8		
RALY	gi|8051631	32.5	15	7			3	11		
Miscellaneous proteins										
RBM7	gi|4503293	30.5		2	3	6	4	4		
LOC51325 (GCFC, fSAP105)	gi|22035565	104.8		19	13	7	38	36		
USP42	gi|79750944	144.2		3	1	2	7	12		
SHARP	gi|14790190	402.2		23	10	6				
SON3 (DBP-5)	gi|21040318	263.7			11	7	27	8		
IGF2BP3 (Koc1)	gi|30795212	63.6		3	1	1	1	2		
TARDBP	gi|6678271	44.6		5	1	1	5			
BAG2 (KiAA0576)	gi|4757834	23.6	10		2	2	5	5		
ZCCHC8	gi|38044290	78.5			6	5	6	6		
NUMA1(NUMA, centrophilin)	gi|71361682	238.1			10	12		5		
DDX21(GURDB, RH-II_GU, GUA)	gi|50659095	87.2		11	15	10		14		
ERH	gi|4758302	12.1		5	3	1				

Proteins identified by LC-MSMS after separation by PAGE in B^{act} complexes formed on both PM5-10 and PM5-20 pre-mRNA, and C complexes formed on PM5 or $MINX_{gg}$ substrates are shown. Proteins not reproducibly detected are summarized in Supplemental Table S1. Proteins generally accepted to be common contaminants, such as tubulins and ribosomal and exosome proteins, are not shown. The presence of a protein is indicated by a number which represents the absolute number of peptides sequenced for that protein in a particular preparation. The presence of a protein in the *S. cerevisiae* B^{act} complex (Fabrizio et al. 2009) is indicated by a dot. The absolute number of peptides sequenced previously for proteins identified by LC-MSMS in affinity-purified human B complexes formed on the PM5 pre-mRNA (Bessonov et al. 2008) is also shown. Proteins are grouped in organizational and/or functional subgroups.
[a]TCERG1 (CA150), FBP11, and NRIP were previously found in the spliceosomal A complex and thus they are designated as "recruited prior to B^{act}."

and PM5–10 exhibiting a nearly identical composition. Consistent with its snRNA composition, the human B^{act} complex contains all U2 and U5 snRNP proteins, with the exception of Dib1/15K that appears to be lost upon activation of the spliceosome (i.e., it is present in B but not B^{act} or C complexes). In addition, based on the number of peptides sequenced by MS as well as the results of immunoblotting (Fig. 3A), U1 and U4/U6 snRNP proteins, including the Lsm proteins are lost or underrepresented (relative to the B complex) in B^{act} complexes. Thus, in humans, the Lsm proteins are destabilized/lost during the B to B^{act} complex transition. These data indicate that in the human spliceosome, the Lsm 2–8 proteins leave the spliceosome just prior to or during activation. Several other proteins are destabilized during the B to B^{act} transition (i.e., more peptides of them were sequenced in B versus B^{act}), including RED, THRAP3, and Smu-1.

In contrast, a number of proteins are recruited or more stably associated with the spliceosome upon its activation. Nearly all hPrp19/CDC5L complex proteins, as well as an additional group operationally defined as hPrp19/CDC5L-related, plus hPrp17, KIAA1604, and SRm300, are more abundant in B^{act}, based on the number of peptides sequenced (Table 1), as well as the results of immunoblotting (Fig. 3A). These proteins appear to be equally abundant in purified C complexes, indicating that they associate first during activation and remain stably associated at least through the first catalytic step of splicing. In contrast, whereas hPrp2, GPKOW, MGC20398, PPIL2, MGC23918, NY-CO-10, RNF113A, and FRG1, as well as two members of the RES complex (SNIP1 and MGC13125), are more abundant in B^{act} versus B, they appear to be lost/destabilized during the B^{act} to C transition. Thus, these proteins appear to be transiently associated with the spliceosome during its activation phase. In addition, a group of 12 proteins (designated in Table 1 as "Detected in B^{act} complex") were specifically detected in our B^{act} complexes, but appear to be present in very low amounts (see Discussion). The presence of the DExH/D-box protein hPrp2 in our purified B^{act} complexes is consistent with the idea that they have not yet undergone catalytic activation, as Prp2 (at least in yeast) is known to dissociate from the spliceosome after catalyzing the remodeling step that yields a catalytically active B* complex (Kim and Lin 1996).

Only very few peptides of known step II splicing factors, like hPrp22, hPrp16, and hSlu7, were detected in B^{act} complexes and immunoblotting confirmed the near absence of hPrp22 in the latter (Fig. 3A). Likewise, a number of proteins previously found to be associated with C but not with B complexes (Table 1, abundant first in C complex) were absent or found only in low amounts in B^{act} complexes (Table 1; Fig. 3A). These include, among many others, the DExD/H-box helicases Abstrakt and DDX35, and the PPIases PPWD1, PPIL3b, and PPIG. Thus, these proteins are recruited and/or their interaction stabilized after spliceosome activation. Finally, a comparison of the number of SF3a and SF3b protein peptides sequenced in all three complexes indicates that SF3a/b proteins are specifically destabilized from the human spliceosome during the B^{act} to C complex transition (Table 1); indeed, immunoblotting confirmed that only low levels of SF3b155 are found in purified C complexes (Fig. 3B). Taken together, these results provide new insights into the recruitment and release of human proteins during the B to B^{act} and B^{act} to C complex transitions.

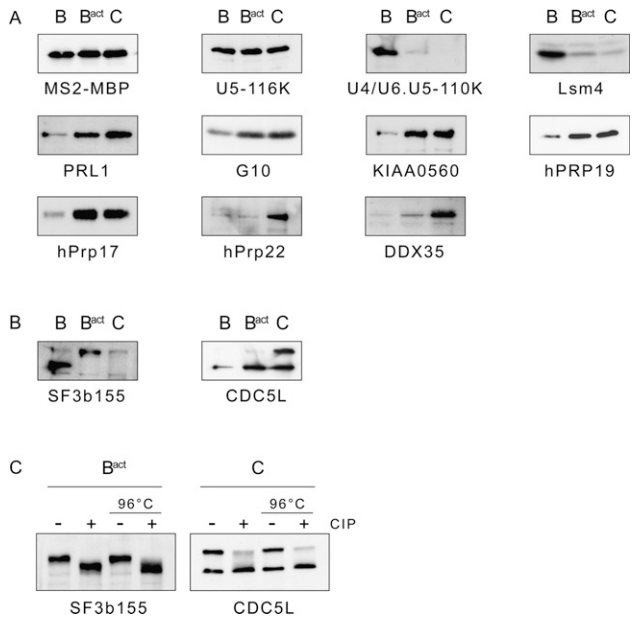

FIGURE 3. Immunoblotting reveals the dynamics of spliceosomal protein association and post-translational modification of SF3b155 and CDC5L. (*A*) B and C complexes formed on PM5 pre-mRNA, and B^{act} complexes formed on PM5-20 pre-mRNA, were affinity purified and their proteins analyzed by Western blotting with the antibodies indicated below or in (*B*) against SF3b155 or CDC5L. Antibodies against MS2-MBP and the U5-116k protein were used to ensure equal loading. (*C*) B^{act} and C complexes were incubated in the absence (−) or presence (+) of calf intestine pyrophosphatase (CIP) directly (*left* two lanes) or after first incubating at 96°C to inactivate endogenous enzymatic activity (*right* two lanes). Immunoblotting was performed with anti-SF3b155 or anti-CDC5L antibodies, as indicated below.

SF3b155 and CDC5L are phosphorylated prior to/during spliceosome activation and step I of splicing, respectively

The SF3b155 protein is phosphorylated concomitantly with or just prior to the first step of splicing (Wang et al. 1998). To test whether SF3b155 phosphorylation occurs already during B^{act} formation or first at a later stage, we performed immunoblotting with proteins from affinity-purified B, B^{act}, and C complexes. A major band that migrated slower than the SF3b155 band detected by anti-SF3b155 antibodies in B complexes, was observed in B^{act} complexes (Fig. 3B). Thus, SF3b155 is quantitatively phosphorylated first in B^{act}

complexes. Consistent with the lower number of peptides sequenced by MS for SF3b155 in C complexes, only very weak immunostaining was observed when C complexes were probed with anti-SF3b155 antibodies (Fig. 3B).

When C complex proteins were separated by SDS-PAGE and subsequently analyzed by MS, peptides specific to the CDC5L protein were unexpectedly detected in two separate regions of the gel. Consistent with this result, when immunoblotting was performed with anti-CDC5L antibodies, two bands were observed when C complexes (but not B or the B^{act}) were analyzed, one of the expected size (92 kDa) and one that migrated significantly slower (Fig. 3B). As MS analyses did not provide any evidence for potential glycosylation, ubiquitinylation or SUMOylation of CDC5L, and CDC5L was previously reported to be phosphorylated in vivo (Bernstein and Coughlin 1997; Graub et al. 2008), we tested whether this slowly migrating form of CDC5L is phosphorylated. For this purpose, we treated C complexes with calf intestine pyrophosphatase (CIP) prior to immunoblotting, and then probed with anti-CDC5L antibodies. After CIP treatment, the intensity of the upper band was clearly reduced, whereas the intensity of the lower band was enhanced, indicating that CDC5L is indeed phosphorylated (Fig. 3C). To rule out that the dephosphorylation of a different C complex protein by CIP stimulates its enzymatic activity, which in turn leads to removal of the CDC5L modification (e.g., deglycosylation or deubiquitinylation), C complexes were incubated at 96°C prior to treating them with CIP, in order to suppress any endogeneous enzymatic activity of the C complex. As shown in the Figure 3C, incubation at 96°C followed by CIP treatment also led to a reduction in the intensity of the higher molecular weight band, strongly supporting the idea that CDC5L is phosphorylated during splicing. Similar results were observed for SF3b155 when B^{act} complexes were treated with CIP and the SF3b155 protein subsequently analyzed by immunoblotting (Fig. 3C). In sum, these data indicate that SF3b155 is phosphorylated concomittant with the activation of the human spliceosome, whereas CDC5L is phosphorylated during/just prior to the first catalytic step of splicing.

Electron microscopy of human B^{act} complexes

To determine the morphology of the human B^{act} complex, affinity-purified complexes assembled on the PM5–20 were subjected to GraFix glycerol gradient ultracentrifugation (Kastner et al. 2008), negatively stained, and analyzed by electron microscopy. The overview images revealed a monodisperse population of particles with a maximum dimension of ~44 nm (Fig. 4A). Unbiased single-particle image-clustering revealed representative class averages (Fig. 4B). Many of the classes look quite similar (left half of Fig. 4B) indicating a preferential orientation of the B^{act} complexes on the carbon film used to support the EM specimens. The characteristic shape of the dominant classes show a cap or hat like main body (oriented upward) and two lower protuberances. One lower protuberance appears to originate from the center of the main body while the other is seen at the right side in these dominant classes. The appearance of this protuberance varies significantly in shape and position in the various classes. The differences seen in the main body, which might arise from slight differences in the orientation of the particles on the carbon film, are less pronounced. Some classes show a nearly round upper outline (column 1) while in others it is more asymmetric (columns 2–5), sloping left and right at different angles, such that the left appears steeper than the right. Within the main body a central stain accumulation is visible predominantly in these dominant views. Some also show a more elongated accumulation of stain, parallel to the left flank and a point-like accumulation of stain on the right (column 5). The central lower protrusion is quite thin and looks somewhat like a hook bent to the left (columns 1–4). In some classes this protuberance overlaps with the heterogeneous protuberance (columns 5–6). In the more rare classes, the two lower domains can hardly be discerned and the views become progressively thinner (columns 7–8). Here, the particle might be viewed from the side or from the top. B^{act} complexes assembled on the PM5–10 pre-mRNA substrate show very similar EM images, and no structural differences could be detected by inspection of the class averages (data not shown).

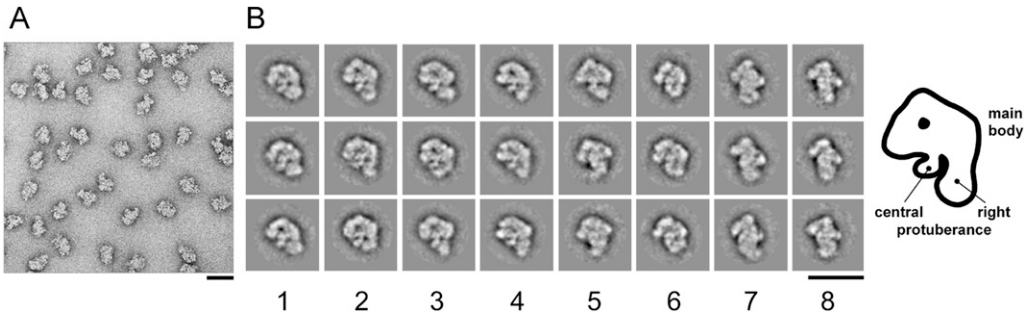

FIGURE 4. Negative stain electron microscopy of affinity purified B^{act} complexes. (*A*) Negative stain EM raw images of human B^{act} complexes formed on the PM5-20 pre-mRNA substrate. (*B*) Selected class averages of spliceosomal B^{act} complexes assembled on the PM5-20 pre-mRNA construct. At the *right*, a schematic drawing corresponding to class averages seen in columns 1–4 is shown. Bar = 50 nm.

Structural dynamics during the B to B^{act} transition

To learn more about the structural dynamics of the spliceosome during its activation, we compared the 2D images of the human B^{act} complexes with those of the human B complex. The spliceosomal B^{act} complex has roughly the same size as the B complex (Fig. 5; Deckert et al. 2006). Nonetheless, their morphology differs considerably. Spliceosomal B complexes are rhombic shaped, with a triangular main body linked to an upper globular domain. While the triangular body exhibits a quite rigid morphology in the various 2D classes, the globular domain shows a high degree of structural heterogeneity. Although both complexes possess a heterogeneous domain, the main part of the B^{act} complex exhibits a more globular shape and therefore has a very different morphology. Thus, consistent with the compositional remodeling that occurs during spliceosome activation, the morphology of the spliceosome during the B to B^{act} transition changes in a similar dramatic fashion.

DISCUSSION

To learn more about the compositional and structural dynamics of the human spliceosome during its activation, we affinity purified human B^{act} complexes formed on a truncated PM5 pre-mRNA, under the same conditions previously used to isolate B and C complexes that were also formed on the PM5 substrate. A comparison of the protein composition of B^{act} complexes with that of the B complex revealed significant compositional changes during the B to B^{act} transition. Post-translational modifications that potentially contribute to activation or the first step of splicing, namely, the phosphorylation of SF3b155 and CDC5L, respectively, were also shown to occur concomittant with B^{act} (in the case of SF3b155) or C complex (in the case of CDC5L) formation. EM analyses of the structure of the B^{act} complex, in comparison with that of B, revealed that the human spliceosome is significantly remodeled during activation. Taken together, these data provide new insights into spliceosomal dynamics in humans during a decisive stage of the splicing process.

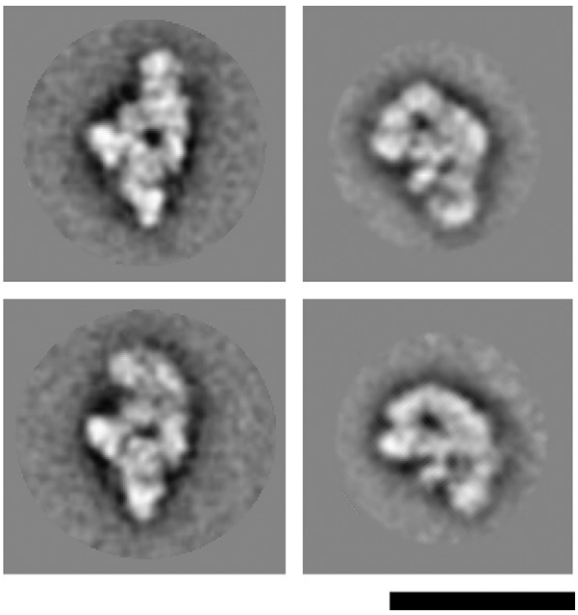

FIGURE 5. Comparison of the EM images of the human B and B^{act} complexes. Typical class averages of the human B (*left* panels) (Deckert et al. 2006) and B^{act} (*right* panels) complexes are shown. Bar = 50 nm.

Human B^{act} complexes can be affinity purified after truncating the PPT tract of a pre-mRNA lacking a 3′ss and 3′ exon

Under standard in vitro splicing conditions with a wild-type pre-mRNA substrate, B^{act} complexes are difficult to discern on native gels, presumably due to the fact that upon activation they rapidly catalyze step 1 of splicing and are thereby converted into the C complex. Previously, it was observed in *S. cerevisiae* that if the pre-mRNA is truncated to just a few nucleotides downstream of the BPS, spliceosome assembly is blocked at the activation stage (Cheng 1994). Very recently, yeast B^{act} complexes were isolated in our laboratory using a pre-mRNA substrate derived from the actin pre-mRNA, whose intron was truncated such that it included only six nucleotides downstream of the BPS (Fabrizio et al. 2009). We tested if a similar approach could be used in order to isolate human B^{act} complexes. Indeed, shortening the PPT of the PM5 pre-mRNA (which also lacks a 3′ss and 3′ exon) stalled splicing after B complex formation but prior to the first catalytic step (Fig. 1), and allowed the subsequent affinity purification of human B^{act} complexes (Fig. 2). The identity of these complexes was confirmed by their RNA content—i.e., they lacked for the most part U1 and U4 snRNA and also the intermediates of the splicing reaction—and was further supported by their protein composition (see also below). That is, previous results in yeast indicated that Prp2 dissociates from the spliceosome after catalyzing the remodeling step that converts B^{act} into a B^* complex (Kim and Lin 1996). MS demonstrated that the hPrp2 and GPKOW proteins, human homologs of Prp2 and Spp2, respectively, are highly abundant in our B^{act} complexes (Table 1), suggesting that they are not yet catalytically active and thus stalled prior to B^* formation. Consistent with the idea that Prp2 leaves the spliceosome just before or during the first catalytic step, hPrp2 and GPKOW were less abundant (based on the number of peptides sequenced) in C versus B^{act} complexes (Table 1). In contrast to our purified B and C complexes, purified human B^{act} spliceosomes were not capable of catalyzing splicing in the presence of micrococcal nuclease (MN)-treated nuclear extract, even when the splicing reaction was additionally supplemented with a 3′ substrate RNA (data not shown). The finding that the hPrp2 protein is enriched in our B^{act} complexes, but nonetheless spliceosomes assembled

on the PM5 pre-mRNAs with a short PPT do not proceed to the first catalytic step, suggests that an unknown factor required to trigger hPrp2 activity is missing in our B^{act} complexes. It is tempting to speculate that a longer polypyrimidine stretch may be required—either directly or as a protein-binding site—to stimulate ATP hydrolysis and/or to support the structural rearrangement of the spliceosome that occurs during the hPrp2-mediated remodeling step.

Previously our lab isolated an activated human spliceosome (formed on an adenovirus pre-mRNA) under stringent conditions via anti-SKIP immunoaffinity chromatography, which was designated the B* complex (Makarov et al. 2002). Although hPrp2 was not detected in these complexes, it is not clear whether these complexes are truly B* and not B^{act} complexes, as they were isolated under conditions (i.e., in the presence of heparin) where hPrp2 could have been stripped away. Furthermore, the SKIP protein is clearly highly abundant in the B^{act} complexes isolated here, further suggesting that the previously isolated complexes may be B^{act} or a mixture of B^{act} plus B* complexes. A comparison of the B^{act} complexes isolated here under physiological conditions with these complexes (to which only very stable components remain bound), reveals that the vast majority of the proteins identified in the latter are also found in the B^{act} complexes described here. Notable exceptions include, PPIL3 (a protein abundant in the C complex), which could thus potentially be recruited first after catalytic activation by Prp2 (i.e., in the B* complex). In contrast, ~40 additional proteins are detected in our B^{act} complexes, suggesting that these proteins are more loosely associated, and thus, for the most part, do not withstand heparin treatment.

Protein dynamics during the B to B^{act} complex transition

At least 30 proteins present in B complexes are destabilized or released from the spliceosome during its activation. These are most notably all U1- and U4/U6-associated proteins plus other snRNP-associated and also non-snRNP proteins (Table 1). For example, proteins such as RED, THRAP3, and several other factors that were abundant in B complexes, are strongly underrepresented or not detected at all in our B^{act} complexes. In yeast, there is evidence that the U6 snRNA-associated Lsm proteins are destabilized upon activation, thereby allowing the base pairing interaction between the U6 snRNA and intron nucleotides near the 5′ss (Chan et al. 2003; Fabrizio et al. 2009). A comparison of the number of peptides sequenced for individual Lsm proteins in our B versus B^{act} and C complexes, as well as immunoblotting with anti-Lsm4 antibodies, indicates that the Lsm proteins are for the most part already absent from B^{act} complexes. Our data therefore support the idea that, similar to yeast, the Lsm proteins are lost in higher eukaryotes during the activation of the spliceosome.

Approximately 35 proteins are recruited to the spliceosome or more stably associated during B^{act} complex formation (Table 1). As discussed above, these include the DExD/H-box helicase hPrp2 and GPKOW. In addition, MGC20398, MGC23918, KIAA1604, RNF113A (all containing various domains known to mediate protein–protein interactions), and two members of the cyclophilin family of peptidyl-prolyl bond *cis/trans* isomerases (PPIases) (PPIL2 and NY-CO-10) appear to be highly abundant. However, the importance of these proteins for splicing in metazoans remains unclear. Homologs of KIAA1604, RNF113A, and NY-CO-10 were detected among *S. cerevisiae* splicing factors suggesting a conserved role for these proteins in splicing. Finally, SRm300 and the RES complex proteins SNIP1 and MGC13125 are also more abundant in B^{act} compared with B.

In addition to these proteins, at least 12 proteins (Table 1, detected in B^{act} complex) were detected specifically in our B^{act} complexes. A relatively low number of peptides were sequenced by MS for most of these proteins, suggesting that they are not abundant components of the B^{act} complex. Indeed, semiquantitative 2D gel analyses performed in our lab indicate that these proteins are present in very low amounts (D. Agafonov and R. Lührmann, in prep.) and they may thus be contaminants. Consistent with this idea, the vast majority of these proteins have never been detected in any human spliceosomal complexes and none are known to function in splicing.

Although proteins of the hPrp19/CDC5L complex and related factors are detected by MS in our purified B complexes, they are first stably recruited at the stage of B^{act} complex formation as indicated by the higher number of peptides sequenced by MS for each of these proteins (Table 1). This finding is in a good agreement with previous observations that the NTC (the yeast counterpart of the hPrp19/CDC5L complex) stably binds to the spliceosome after U4 dissociation and is required for spliceosome activation (Chan et al. 2003; Chan and Cheng 2005). Among the proteins most prominent first in the B^{act} complex, was hPrp17, the human homolog of the nonessential, yeast second-step factor Prp17. The detection of hPrp17 in our B^{act} complexes, but not other step II factors, is consistent with recent results obtained in yeast suggesting that Prp17 functions in both steps of splicing (Sapra et al. 2008).

Protein dynamics during the B^{act} to C complex transition

Approximately 20 proteins dissociate or are destabilized from the spliceosome during the B^{act} to C complex transition (Table 1). Interestingly, among these are several proteins recruited to the B^{act} complex including: hPrp2, GPKOW, RNF113A, MGC23918, MGC20398, PPIL2, and NY-CO-10. The fact that these proteins appear to be solely present or enriched in B^{act} versus B and C complexes suggests they play a potential role in the spliceosome activation process. Whereas such a role has been already shown for Prp2 and Spp2 (the yeast homolog of GPKOW) in *S. cerevisiae* (see above), a role

for other B^{act} specific proteins in pre-mRNA splicing remains to be demonstrated. SF3a and SF3b complex proteins are also destabilized from the spliceosome during the B^{act} to C transition, as evidenced by MS analysis (Table 1) and immunoblotting with anti-SF3b155 antibodies (Fig. 3). SF3a and SF3b play an essential role in tethering the U2 snRNP to the branch site, and contacts between the pre-mRNA branch site and some SF3b components, such as p14, appear to persist at least up to the first step of splicing (MacMillan et al. 1994). Prior to the second step of splicing, the branch adenosine is thought to be removed from the active site of the spliceosome and replaced by the 3′ss (for review, see Smith et al. 2008). A recent report indicates that in yeast the second step of splicing can proceed in the absence of U2/BPS base pairing (Smith et al. 2007). The U2- associated SF3a and SF3b proteins are bound to the spliceosome in a salt resistant manner prior to C complex formation (data not shown). Moreover, recent studies in yeast demonstrated that ATP hydrolysis by Prp2 destabilizes the interaction of the SF3a and SF3b proteins with the spliceosome (Warkocki et al. 2009; Lardelli et al. 2010). Thus, at least in yeast, SF3a and SF3b interactions with the spliceosome are remodeled already prior to the first step of splicing. Although SF3a and SF3b play essential roles early in the splicing reaction, our data are consistent with the idea that they may not be required after the first catalytic step.

A number of proteins previously detected in C complexes (Bessonov et al. 2008) were absent or underrepresented in our B^{act} complexes and were thus recruited during the B^{act} to C transition. These included, among others, the second-step factors hPrp22 and hSlu7, and the DExD/H-box helicases Abstrakt and DDX35, whose function in splicing is not known. A number of cyclophilins, a group of proteins that belong to the family of peptidyl-prolyl bond *cis/trans* isomerases (PPIases), are detected in human spliceosomal complexes. These include PPIH, Cyp-E, PPIL1, PPIL2, NY-CO-10, PPIL3b, PPWD1, and PPIG. Only one of these proteins, namely, PPIH, or the U4/U6 snRNP-associated 20k protein, is present in B complexes, but absent from B^{act} and C complexes. Cyp-E, PPIL2, and NY-CO-10 appear to be abundantly present first at the B^{act} complex stage. Cyp-E and PPIL1, both Prp19-related proteins, appear to be associated with the spliceosome throughout both catalytic steps as they were detected in B^{act} and C complexes (Table 1) and in the post-spliceosomal 35S U5 snRNP (Makarov et al. 2002). PPIL3b, PPWD1, and PPIG are almost exclusively detected in the C complex, indicating that they are likely recruited after or concomitant with the first step of splicing (Table 1). The role of cyclophilins in the spliceosome is not clear. As prolyl isomerases, they could aid in the folding and activation of proline containing splicing factors. To date, the only protein of this group that was shown to be important for splicing is PPIH (Horowitz et al. 2002), but its enzymatic target remains unknown. It thus remains to be determined whether the other cyclophilins are essential for splicing or whether they play a more auxiliary role, for example, by accelerating splicing via promoting the proper conformation of certain proteins.

Phosphorylation of SF3b155 and CDC5L occurs concomittant with spliceosome activation and step I of splicing, respectively

Numerous studies have shown that reversible phosphorylation plays an important role in pre-mRNA splicing (for review, see Soret and Tazi 2003). Previously, it was shown that the SF3b155 protein is phosphorylated prior to or during the first step of splicing (Wang et al. 1998). Here, we demonstrate that SF3b155 is quantitatively phosphorylated in our B^{act} complexes that are stalled at a very defined stage, namely, prior to Prp2 action (Fig. 3). The CDC5L protein, which also plays a role in cell cycle progression (Bernstein and Coughlin 1998), is phosphorylated first upon formation of the C complex and thus after catalytic activation of the spliceosome (Fig. 3). Previous studies demonstrated that human CDC5L is phosphorylated at at least nine sites in vivo, and suggested that the phosphorylation of threonines at positions 411 and 438 are required for the first step of splicing in vitro (Graub et al. 2008). Based on our data it is thus tempting to hypothesize that the phosphorylation of CDC5L plays an important role in the first step of splicing, whereas phosphorylation of SF3b155 may play an important role in spliceosome activation. However, further studies are required to elucidate the exact role of the phosphorylation or/and dephosphorylation of these proteins in splicing.

Comparison of the protein composition of human and yeast B^{act} complexes

The protein compositions of affinity-purified *S. cerevisiae* spliceosomal B, B^{act}, and C complexes were recently determined by MS (Fabrizio et al. 2009). Altogether ~90 proteins were identified in yeast spliceosomes, nearly all of which have human homologs. Thus, comparison of the composition of the human and yeast spliceosomal complexes suggests a high degree of conservation of the core splicing machinery between human and yeast (Table 1). Indeed, although yeast B^{act} complexes lack SR and hnRNP proteins and many other factors found in human B^{act} complexes, human homologs of nearly all proteins found in yeast B^{act} complexes (with the exception of Ntc20) are also found in human B^{act} complexes (Table 1). Like the human B^{act} complex, Prp2 was enriched in the affinity-purified yeast B^{act} complexes, indicating that both B^{act} complexes are stalled prior to the Prp2 action. Homologs of most of the other proteins first enriched in human B^{act} complexes are also found in yeast, including GPKOW (Spp2 in yeast), KIAA1604 (Cwc22), NY-CO-10 (Cwc27), RNF113A (Cwc24), and SRm300 (Cwc21) (Table 1). Prp17 is also first highly abundant at the time of B^{act} formation in yeast.

Although the human hPrp19/CDC5L complex and its yeast counterpart, namely, the NTC, are compositionally different (i.e., they share three homologous proteins Prp19/hPrp19, Cef1/CDC5L, and Snt309/SPF27, but the NTC contains additionally Syf1, Syf2, Clf1, Isy1, and Ntc20) (Chen et al. 2002; Makarova et al. 2004), proteins of the NTC are also first abundant (and thus presumably stably associated) in the yeast B^{act} complex. Furthermore, yeast proteins homologous to other human hPrp19/CDC5L components, such as Cwc15/AD002 and Prp46/PRL1, are also stably integrated into the yeast B^{act} complex. The same is true for several other yeast proteins, which were previously shown be associated with Cef1, the yeast homolog of CDC5L (Ohi et al. 2002), and their human counterparts that are operationally defined as hPrp19-related.

Taken together, these data reveal conservation of the core splicing machinery at the stage of activation. Many of the additional proteins found in human B^{act} complexes do not have homologs in yeast and/or are involved in regulated splicing such as SR proteins, whereas others are likely present in substoichiometric amounts, based on the low number of peptides sequenced. Although the number of splicing factors associated with purified human spliceosomes is much larger than those found in yeast spliceosomes, the dynamics of protein recruitment and dissociation during spliceosome activation is largely conserved between human and yeast. This indicates that the observed compositional remodeling is an evolutionarily conserved design principle of the spliceosome.

Human and yeast B^{act} complexes have a similar morphology

Recently, B, C, and B^{act} spliceosomal complexes were purified from the yeast *S. cerevisiae* and their structure analyzed by EM after GraFix treatment (Fabrizio et al. 2009). All three yeast spliceosomal complexes exhibited a different morphology as judged by 2D class averages. The typical views of the yeast B^{act} complex, which was also assembled on a pre-mRNA with a truncated PY tract, show in the most frequent images a compact slightly asymmetrical main body with a foot-like protrusion pointing downward (Fig. 6, left). If the image classes of the human B^{act} complex (Fig. 6, right) are compared with those of the yeast complex, a large extent of similarity can be recognized. Both show a quite similar main body that appears in typical views with a steep slope at the left side and a more shallow one on the other side. Similar to yeast, some views of the human particle also show on the left a more elongated accumulation of stain running parallel to the left flank and on the right a more point-like stain accumulation. Like the human particle, the yeast B^{act} complex has a central lower protrusion, but it appears more massive in the yeast particle. The most obvious difference between the two B^{act} complexes is the heterogeneous protuberance at the lower right side that is present in the human complex but appears to be completely missing in the yeast complex. Overall, the human B^{act} complex is somewhat larger than the yeast B^{act} complex, with, for example, the width of the main body reaching 31 ± 1 nm in the yeast complex versus 34 ± 1 nm in the human complex. This is consistent with the presence of additional proteins in the latter. However, based on the low number of peptides sequenced for many of those proteins solely found in the human B^{act} complex (Table 1), a large number of these proteins are likely present in substoichiometric amounts and are thus not expected to contribute to the mass of the B^{act}

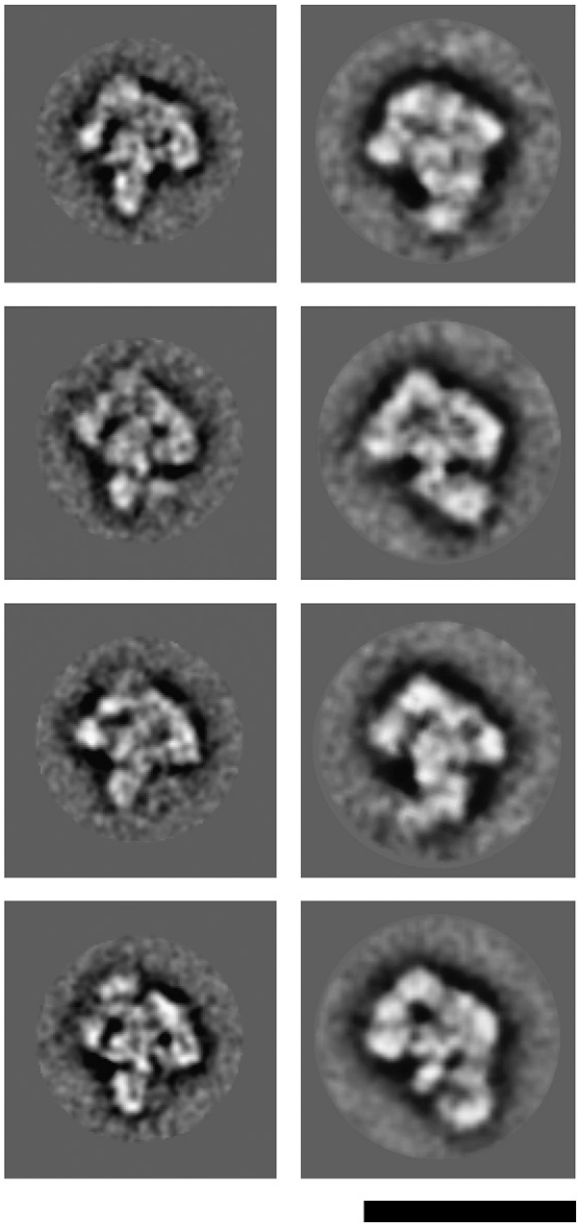

FIGURE 6. The human and yeast B^{act} complexes share a similar morphology. Typical class averages of the human (*right* panels) and yeast (*left* panels) B^{act} complexes (Fabrizio et al. 2009), visualized by electron microscopy after negative staining, are shown. Bar = 50 nm.

complex observed under the electron microscope. In summary, it can be concluded from these structural comparisons that, like the B complex, the overall architecture of the human and *S. cerevisiae* B^{act} spliceosomal complex is similar, suggesting that many of the higher order interactions among spliceosomal components, as well as their dynamics, are also largely conserved. However, future 3D reconstructions of the B^{act} complex will be needed to conclusively elucidate morphological similarities and differences between the human and yeast complexes.

MATERIALS AND METHODS

In vitro splicing and native agarose gel electrophoresis

The polypyrimidine tract of the PM5 pre-mRNA substrate (Bessonov et al. 2008) was truncated to different lengths using standard PCR techniques. Uniformly [^{32}P]-labeled, m^{7}G(5′)ppp(5′) G-capped pre-mRNAs were synthesized in vitro by SP6 runoff transcription and gel purified. HeLa nuclear extract was prepared as previously described (Dignam et al. 1983). A typical splicing reaction contained 20 nM of ^{32}P-labeled pre-mRNA and 30%–50% HeLa nuclear extract in buffer containing 3 mM $MgCl_2$, 65 mM KCl, 20 mM HEPES–KOH pH 7.9, 2 mM ATP, and 20 mM creatine phosphate, and was incubated at 30°C for the times indicated. RNA was then isolated and analyzed by denaturing PAGE on a 7M urea, 10% polyacrylamide gel, followed by autoradiography. To analyze splicing complex formation, heparin was added to 18-μL aliquots of the splicing reaction to a final concentration of 0.125 mg/mL and the mixtures were incubated for 1 min at 30°C before addition of 2 μL of agarose loading buffer (30% glycerol. 0.05% xylene cyanol, 100 mM Tris, pH 8.3, 83 mM borate, 1 mM EDTA). Complexes were analyzed on a 1.5% low melting agarose gel and visualized by autoradiography.

MS2 affinity purification of spliceosomal complexes and mass spectrometry

C complexes formed on PM5 or $MINX_{GG}$ pre-mRNA substrates were purified by MS2–MBP affinity selection as described previously (Bessonov et al. 2008; Golas et al. 2010). B^{act} complexes were also isolated using the MS2–MBP-affinity selection approach essentially as described previously (Bessonov et al. 2008). Briefly, PM5–20 or PM5–10 pre-mRNA was incubated with a 20-fold molar excess of purified MS2–MBP fusion protein. Then, a 12-mL standard splicing reaction was performed for 150 min with the MS2–MBP bound pre-mRNA. A 30-fold molar excess of DNA oligonucleotide complementary to nucleotides −6 to −18 (relative to the 5′ss) of the PM5 substrate was added and the reaction was incubated at 30°C for an additional 20 min. Spliceosomal complexes were size fractionated by 10%–30% glycerol gradient centrifugation and the distribution of the ^{32}P-labeled pre-mRNA was determined by Cherenkov counting. 45S peak fractions were pooled and loaded onto an amylose agarose column (New England Biolabs) and after washing, spliceosomal complexes were eluted with 20 mM maltose in G-buffer (20 mM HEPES, pH 7.9, 150 mM NaCl, 1.5 mM $MgCl_2$). RNA was recovered from the eluted B^{act} complexes, analyzed on a 7M urea–10% polyacrylamide gel, and visualized by silver staining and autoradiography. Proteins were recovered, analyzed by SDS-PAGE, and stained with Coomassie. Proteins were identified by LC-MSMS as described previously (Bessonov et al. 2008).

Immunoblotting and CIP digestions

Proteins were separated by SDS-PAGE on an 8% polyacrylamide gel, transferred to Hybond P membrane and immunostained using an ECL detection kit (Pierce). Antibodies against the following human proteins were used: U5-116K/Snu114 (Fabrizio et al. 1997); SF3b155 (Will et al. 2001); U4/U6.U5-110K (Makarova et al. 2001); CDC5L, KIAA1604, Lsm4, and hPrp19 (Makarova et al. 2004); PRL1, DDX35, hPrp22, and hPrp17 (Bessonov et al. 2008); MS2-MBP (Abcam); G10 (raised against aa 32 to 45). Digestion with calf intestinal phosphatase (NEB) was performed according to the manufacturer's protocol.

Electron microscopy (EM)

For EM, spliceosomal complexes eluted from the amylose column were subjected to an additional GraFix glycerol gradient ultracentrifugation (Kastner et al. 2008), which combines mild chemical fixation and ultracentrifugation. Briefly, 5 pmol of spliceosomes were loaded onto a gradient containing 10%–30% (v/v) glycerol and 0%–0.1% (w/v) glutaraldehyde in G-buffer. The gradients were centrifuged for 1.5 h at 60,000 rpm (~489,000*g*) in a TH660 rotor at 4°C. Fractions of 175 μL were collected from the bottom using a Brandel BR-184X fractionator. Peak fractions were identified by scintillation counting and analyzed by negative staining except that the specimen was stored and imaged at ambient temperature (Golas et al. 2003). Micrographs were taken at 160 kV and 122,000× magnification with a CM200 FEG microscope at twofold binning on a 4k × 4k CCD camera. Individual particle images were selected from the CCD images using Signature (Chen and Grigorieff 2007). Approximately 35,000 single particle images were selected, and after iterative image processing they were classified into 1600 classes out of which the representative classes are shown. Iterative rounds of image processing were performed in the context of the software package IMAGIC-5 (van Heel et al. 1996). The 2D image processing was performed until the result was stable. This included alignment using resampling to polar coordinates (Sander et al. 2003) and multivariate statistical classification (van Heel 1984).

SUPPLEMENTAL MATERIAL

Supplemental material can be found at http://www.rnajournal.org.

ACKNOWLEDGMENTS

We are grateful to T. Conrad and H. Kohansal for preparing HeLa cell nuclear extract, and M. Raabe, J. Lehne, and U. Plessmann for excellent help in MS analysis. We thank B. Kastner and Z. Warkocki for helpful comments on the manuscript. This work was supported by a YIP grant from EURASNET to H.U., a grant from the Federal Ministry of Education and Research (BMBF), Germany, the Sixth Framework Programme of the European Union via the Integrated

Project 3D repertoire to H.S., and by a grant from the European Commission (EURASNET-518238) to R.L.

Received September 8, 2010; accepted September 23, 2010.

REFERENCES

Bartels C, Klatt C, Lührmann R, Fabrizio P. 2002. The ribosomal translocase homologue Snu114p is involved in unwinding U4/U6 RNA during activation of the spliceosome. *EMBO Rep* **3:** 875–880.

Behzadnia N, Golas MM, Hartmuth K, Sander B, Kastner B, Deckert J, Dube P, Will CL, Urlaub H, Stark H, et al. 2007. Composition and three-dimensional EM structure of double affinity-purified, human prespliceosomal A complexes. *EMBO J* **26:** 1737–1748.

Bernstein HS, Coughlin SR. 1997. Pombe Cdc5-related protein. A putative human transcription factor implicated in mitogen-activated signaling. *J Biol Chem* **272:** 5833–5837.

Bernstein HS, Coughlin SR. 1998. A mammalian homolog of fission yeast Cdc5 regulates G2 progression and mitotic entry. *J Biol Chem* **273:** 4666–4671.

Bessonov S, Anokhina M, Will CL, Urlaub H, Lührmann R. 2008. Isolation of an active step I spliceosome and composition of its RNP core. *Nature* **452:** 846–850.

Brenner TJ, Guthrie C. 2005. Genetic analysis reveals a role for the C terminus of the *Saccharomyces cerevisiae* GTPase Snu114 during spliceosome activation. *Genetics* **170:** 1063–1080.

Chan SP, Cheng SC. 2005. The Prp19-associated complex is required for specifying interactions of U5 and U6 with pre-mRNA during spliceosome activation. *J Biol Chem* **280:** 31190–31199.

Chan SP, Kao DI, Tsai WY, Cheng SC. 2003. The Prp19p-associated complex in spliceosome activation. *Science* **302:** 279–282.

Chen CH, Yu WC, Tsao TY, Wang LY, Chen HR, Lin JY, Tsai WY, Cheng SC. 2002. Functional and physical interactions between components of the Prp19p-associated complex. *Nucleic Acids Res* **30:** 1029–1037.

Chen JZ, Grigorieff N. 2007. SIGNATURE: A single-particle selection system for molecular electron microscopy. *J Struct Biol* **157:** 168–173.

Chen JY, Stands L, Staley JP, Jackups RR Jr, Latus LJ, Chang TH. 2001. Specific alterations of U1-C protein or U1 small nuclear RNA can eliminate the requirement of Prp28p, an essential DEAD box splicing factor. *Mol Cell* **7:** 227–232.

Cheng SC. 1994. Formation of the yeast splicing complex A1 and association of the splicing factor PRP19 with the pre-mRNA are independent of the 3′ region of the intron. *Nucleic Acids Res* **22:** 1548–1554.

Deckert J, Hartmuth K, Boehringer D, Behzadnia N, Will CL, Kastner B, Stark H, Urlaub H, Luhrmann R. 2006. Protein composition and electron microscopy structure of affinity-purified human spliceosomal B complexes isolated under physiological conditions. *Mol Cell Biol* **26:** 5528–5543.

Dignam JD, Lebovitz RM, Roeder RG. 1983. Accurate transcription initiation by RNA polymerase II in a soluble extract from isolated mammalian nuclei. *Nucleic Acids Res* **11:** 1475–1489.

Fabrizio P, Laggerbauer B, Lauber J, Lane WS, Lührmann R. 1997. An evolutionarily conserved U5 snRNP-specific protein is a GTP-binding factor closely related to the ribosomal translocase EF-2. *EMBO J* **16:** 4092–4106.

Fabrizio P, Dannenberg J, Dube P, Kastner B, Stark H, Urlaub H, Lührmann R. 2009. The evolutionarily conserved core design of the catalytic activation step of the yeast spliceosome. *Mol Cell* **36:** 593–608.

Golas MM, Sander B, Will CL, Lührmann R, Stark H. 2003. Molecular architecture of the multiprotein splicing factor SF3b. *Science* **300:** 980–984.

Golas MM, Sander B, Bessonov S, Grote M, Wolf E, Kastner B, Stark H, Lührmann R. 2010. 3D Cryo-EM structure of an active step I spliceosome and localization of its catalytic core. Mol. Cell. (in press).

Graub R, Lancero H, Pedersen A, Chu M, Padmanabhan K, Xu XQ, Spitz P, Chalkley R, Burlingame AL, Stokoe D, et al. 2008. Cell cycle-dependent phosphorylation of human CDC5 regulates RNA processing. *Cell Cycle* **7:** 1795–1803.

Herold N, Will CL, Wolf E, Kastner B, Urlaub H, Lührmann R. 2009. Conservation of the protein composition and electron microscopy structure of *Drosophila melanogaster* and human spliceosomal complexes. *Mol Cell Biol* **29:** 281–301.

Horowitz DS, Lee EJ, Mabon SA, Misteli T. 2002. A cyclophilin functions in pre-mRNA splicing. *EMBO J* **21:** 470–480.

Jurica MS, Moore MJ. 2003. Pre-mRNA splicing: Awash in a sea of proteins. *Mol Cell* **12:** 5–14.

Jurica MS, Licklider LJ, Gygi SR, Grigorieff N, Moore MJ. 2002. Purification and characterization of native spliceosomes suitable for three-dimensional structural analysis. *RNA* **8:** 426–439.

Kastner B, Fischer N, Golas MM, Sander B, Dube P, Boehringer D, Hartmuth K, Deckert J, Hauer F, Wolf E, et al. 2008. GraFix: sample preparation for single-particle electron cryomicroscopy. *Nat Methods* **5:** 53–55.

Kim SH, Lin RJ. 1996. Spliceosome activation by PRP2 ATPase prior to the first transesterification reaction of pre-mRNA splicing. *Mol Cell Biol* **16:** 6810–6819.

Laggerbauer B, Achsel T, Lührmann R. 1998. The human U5-200kD DEXH-box protein unwinds U4/U6 RNA duplices in vitro. *Proc Natl Acad Sci* **95:** 4188–4192.

Lardelli RM, Thompson JX, Yates JR III, Stevens SW. 2010. Release of SF3 from the intron branchpoint activates the first step of pre-mRNA splicing. *RNA* **16:** 516–528.

MacMillan AM, Query CC, Allerson CR, Chen S, Verdine GL, Sharp PA. 1994. Dynamic association of proteins with the pre-mRNA branch region. *Genes Dev* **8:** 3008–3020.

Makarov EM, Makarova OV, Urlaub H, Gentzel M, Will CL, Wilm M, Lührmann R. 2002. Small nuclear ribonucleoprotein remodeling during catalytic activation of the spliceosome. *Science* **298:** 2205–2208.

Makarova OV, Makarov EM, Lührmann R. 2001. The 65 and 110 kDa SR-related proteins of the U4/U6.U5 tri-snRNP are essential for the assembly of mature spliceosomes. *EMBO J* **20:** 2553–2563.

Makarova OV, Makarov EM, Urlaub H, Will CL, Gentzel M, Wilm M, Lührmann R. 2004. A subset of human 35S U5 proteins, including Prp19, function prior to catalytic step 1 of splicing. *EMBO J* **23:** 2381–2391.

Nilsen TW. 1998. RNA–RNA interactions in nuclear pre-mRNA splicing. In *RNA structure and function* (ed. RW Simons and M Grunberg-Manago), pp. 279–308. Cold Spring Harbor Press, Cold Spring Harbor, NY.

Ohi MD, Link AJ, Ren L, Jennings JL, McDonald WH, Gould KL. 2002. Proteomics analysis reveals stable multiprotein complexes in both fission and budding yeasts containing Myb-related Cdc5p/Cef1p, novel pre-mRNA splicing factors, and snRNAs. *Mol Cell Biol* **22:** 2011–2024.

Raghunathan PL, Guthrie C. 1998. RNA unwinding in U4/U6 snRNPs requires ATP hydrolysis and the DEIH-box splicing factor Brr2. *Curr Biol* **8:** 847–855.

Roy J, Kim K, Maddock JR, Anthony JG, Woolford JL Jr. 1995. The final stages of spliceosome maturation require Spp2p that can interact with the DEAH box protein Prp2p and promote step 1 of splicing. *RNA* **1:** 375–390.

Sander B, Golas MM, Stark H. 2003. Corrim-based alignment for improved speed in single-particle image processing. *J Struct Biol* **143:** 219–228.

Sapra AK, Khandelia P, Vijayraghavan U. 2008. The splicing factor Prp17 interacts with the U2, U5 and U6 snRNPs and associates with the spliceosome pre- and post-catalysis. *Biochem J* **416:** 365–374.

Silverman EJ, Maeda A, Wei J, Smith P, Beggs JD, Lin RJ. 2004. Interaction between a G-patch protein and a spliceosomal DEXD/H-box ATPase that is critical for splicing. *Mol Cell Biol* **24:** 10101–10110.

Small EC, Leggett SR, Winans AA, Staley JP. 2006. The EF-G-like GTPase Snu114p regulates spliceosome dynamics mediated by Brr2p, a DExD/H box ATPase. *Mol Cell* **23:** 389–399.

Smith DJ, Query CC, Konarska MM. 2007. *trans*-splicing to spliceosomal U2 snRNA suggests disruption of branch site-U2 pairing during pre-mRNA splicing. *Mol Cell* **26:** 883–890.

Smith DJ, Query CC, Konarska MM. 2008. "Nought may endure but mutability": Spliceosome dynamics and the regulation of splicing. *Mol Cell* **30:** 657–666.

Soret J, Tazi J. 2003. Phosphorylation-dependent control of the pre-mRNA splicing machinery. *Prog Mol Subcell Biol* **31:** 89–126.

Staley JP, Guthrie C. 1998. Mechanical devices of the spliceosome: Motors, clocks, springs, and things. *Cell* **92:** 315–326.

Staley JP, Guthrie C. 1999. An RNA switch at the 5′ splice site requires ATP and the DEAD box protein Prp28p. *Mol Cell* **3:** 55–64.

van Heel M. 1984. Multivariate statistical classification of noisy images (randomly oriented biological macromolecules). *Ultramicroscopy* **13:** 165–183.

van Heel M, Harauz G, Orlova EV, Schmidt R, Schatz M. 1996. A new generation of the IMAGIC image processing system. *J Struct Biol* **116:** 17–24.

Wahl MC, Will CL, Luhrmann R. 2009. The spliceosome: Design principles of a dynamic RNP machine. *Cell* **136:** 701–718.

Wang C, Chua K, Seghezzi W, Lees E, Gozani O, Reed R. 1998. Phosphorylation of spliceosomal protein SAP 155 coupled with splicing catalysis. *Genes Dev* **12:** 1409–1414.

Warkocki Z, Odenwälder P, Schmitzova J, Platzmann F, Stark H, Urlaub H, Ficner R, Fabrizio P, Lührmann R. 2009. Reconstitution of both steps of *Saccharomyces cerevisiae* splicing with purified spliceosomal components. *Nat Struct Mol Biol* **16:** 1237–1243.

Will CL, Schneider C, MacMillan AM, Katopodis NF, Neubauer G, Wilm M, Lührmann R, Query CC. 2001. A novel U2 and U11/U12 snRNP protein that associates with the pre-mRNA branch site. *EMBO J* **20:** 4536–4546.

Characterization of purified human B^{act} spliceosomal complexes reveals compositional and morphological changes during spliceosome activation and first step catalysis

Sergey Bessonov, Maria Anokhina, Andrius Krasauskas, et al.

RNA 2010 16: 2384-2403 originally published online October 27, 2010
Access the most recent version at doi:10.1261/rna.2456210